Supporting Information

Heisler et al. 10.1073/pnas.1304301111

SI Materials and Methods

Constructs. Sequences coding for PSD-95/SAP90/DLG/ZO-1 (PDZ) domain PDZ1 (aa1–154), PDZ2 (aa140–256), PDZ3 (aa242–473), and PDZ1-3 (aa1–473) of glutamate receptor interacting protein 1 (GRIP1) were separately subcloned as an *EcoRI-SalI* fragment into pGilda (Origene) and used as bait for yeast two-hybrid analysis. A truncated form of *N*-cadherin containing aa102–906 was subcloned as an *EcoRI-XhoI* fragment into pJG4-5 (Origene) and used as prey for yeast two-hybrid analysis. Additional truncation mutants (aa747–906, aa752–774, aa775–791, aa792–811, aa812–847, or 848–906) of *N*-cadherin were amplified from pJG4-5-*N*-cadherin–aa102–906 and cloned into pJG4-5 as *EcoRI-XhoI* fragments. The kinesin motor protein KIF5C construct fused with GFP (GFP-KIF5C) was a kind gift from Michelle Peckham (University of Leeds, Leeds, United Kingdom).

For the plasmid encoding a dominant-negative KIF5C with truncated motor domain (GFP-KIF5CΔMD), aa322–956 of KIF5C were amplified from a rat brain cDNA library and subcloned as a *HindIII-KpnI* fragment into the EGFP-C3 vector (Clontech). To generate pmCherry-KIF5C and pmCherry-KIF5CΔMD, the mCherry sequence was amplified from pmCherry (Clontech), and GFP sequences of either GFP-KIF5C or GFP-KIF5CΔMD were replaced by the mCherry sequence, using *AgeI* and *SacI* restriction sites.

For GFP-GRIP1, full-length GRIP1 cDNA was amplified from a rat brain cDNA library and cloned into the EGFP-C1 vector (Clontech) as a *BglII-SalI* fragment. The mRFP sequence was amplified from pmRFP-N1 (a kind gift from Roger Tsien, Department of Pharmacology, Department of Chemistry and Biochemistry, University of California, San Diego, CA) as an *AgeI-EcoRI* fragment and exchanged with the EGFP fragment in GFP-GRIP1 [monomeric red fluorescent protein (mRFP)-GRIP1]. To generate GFP-GRIP1-PDZ2 and GFP-GRIP1-PDZ4-5, nucleotides coding for aa140–256 (PDZ2) or aa441–655 (PDZ4-5) of GRIP1 were amplified from a rat brain cDNA library and cloned as *BglII-PstI* and *HindIII-KpnI* fragments into pEGFP-C1 (Clontech), respectively. To generate GFP-GluA2-dn, nucleotides coding for aa853–883 (C terminus, compare with refs. 1 and 2) of GluA2 were amplified from pEGFP-GluA2 and cloned as a *SacI-SalI* fragment into pEGFP-C1 (Clontech). To generate mRFP-*N*-cadherin, the mRFP sequence was amplified from pmRFP-N1 and used to replace the Venus sequence in pCXN2-*N*-cadherin-Venus (a kind gift from Hidekazu Tanaka, Department of Pharmacology, Osaka University Medical School, Osaka, Japan), using *XhoI* and *BglII* restriction sites. To generate GFP-N-cadherin-dominant negative (NCAD-dn), nucleotides coding for aa775–791 on *N*-cadherin were subcloned from pJG4-5-*N*-cadherin-aa775–791 into pEGFP-C2 as an *EcoRI-XhoI* fragment.

The GluA2 construct fused to Myc and GFP (GFP-GluA2) was a kind gift from Peter Seeburg (Max Plank Institute for Medical Research, Heidelberg, Germany). The GluA2 construct fused to GFP used for live imaging experiments (GFP-GluA2) was a kind gift from Daniel Choquet (Interdisciplinary Institute for Neuroscience, Bordeaux, France). All constructs were verified by dideoxy sequencing.

Antibodies. The following antibodies were used for immunoprecipitation (IP) and Western blotting (WB): rabbit anti-GFP [2–4 μg (IP) and 1:4,000 (WB); Invitrogen]; mouse anti-GluA2 [4 μg (IP) and 1:3,000 (WB); Chemicon]; rabbit anti-GluA2 [1:3,000 (WB); Chemicon]; rabbit anti-GRIP1 [4 μg (IP) and 1:3,000 (WB); Upstate, Lake Placid, NY]; mouse anti-pan Kinesin Heavy Chain [1:3,000 (WB); Millipore]; rabbit anti-KIF5C [4 μg (IP) and 1:2,000 (WB); Thermo Scientific]; mouse anti-*N*-cadherin [2 μg (IP) and 1:3,000 (WB); BD Biosciences]; mouse anti-Neuroligin1 [1:1,000 (WB); Synaptic System]; mouse anti-Sec8 [4 μg (IP) and 1:3,000 (WB); BD Biosciences]; mouse anti-TRPC1 [1:1,000 (WB); Santa Cruz Biotechnology]; guinea pig anti-Synaptophysin [1:5,000 (WB); Synaptic Systems]; mouse unspecific IgG and rabbit unspecific IgG [both 4 μg (IP); Sigma]; peroxidase-conjugated donkey anti-mouse and donkey anti-rabbit [1:15,000 for mouse and 1:20,000 for rabbit (WB); Dianova].

The following antibodies were used for immunofluorescence: mouse anti-GluA2 (1:1,000; Chemicon); rabbit anti-GRIP1 (1:1,000; Upstate, Lake Placid); goat anti-GRIP1 (1:25; Santa Cruz Biotechnology); rabbit anti-KIF5C (1:1,000; Thermo Scientific); mouse anti-MAP2 (1:5,000; Sigma); mouse anti-*N*-cadherin (1:1,000; BD Biosciences); mouse anti-*N*-cadherin (1:1,000; Sigma); rabbit anti-*N*-cadherin (1:100; Cell Signaling Technologies); rabbit anti-Rab6A (1:100; Sigma); mouse anti-synaptic vesicle (SV2, 1:500; Hybridoma Bank); guinea pig anti-Synaptophysin (1:1,000; Synaptic Systems); Alexa Fluor 488 conjugated donkey anti-mouse and donkey anti-rabbit (both 40μg/mL; Invitrogen); CY3- or CY5-conjugated donkey anti-mouse or donkey anti-rabbit (all 1:1,000; Dianova).

Yeast Two-Hybrid Screening. The Matchmaker LexA Yeast Two-Hybrid system (Clontech) and a rat brain cDNA library (Origene) were used for protein–protein interaction screening. Interaction of bait (pGilda) and prey (pJG4-5) fusions were assayed by activation of the *LEU2* and *lacZ* reporter genes, as previously described (3). Plasmid DNA of positive clones was recovered, and inserts were analyzed by dideoxy sequencing.

Cell Culture and Transfection. Primary cultures of hippocampal neurons were prepared from mice at P0 or E16, as previously described (4). Cells cultured between 9 and 12 d in vitro (DIV9-12) were used for transfection with a calcium phosphate coprecipitation method (4). HEK293 cells were grown to 60% confluency before transfection, using the calcium phosphate coprecipitation protocol.

Differential Centrifugation and Coimmunoprecipitation. Mice or rat brains of five P10 animals were dissected in ice-cold PBS and homogenized in IM-Ac buffer (20 mM Hepes, 100 mM KCl, 5 mM EGTA, and 5 mM $MgCl_2$ at pH 7.2) with freshly added protease inhibitor mixture (Roche), 1 mM PMSF, 5 mM DTT, and 2 mM Mg-ATP (all Sigma). The homogenate was centrifuged at 1,000 × *g* for 10 min, and the resulting postnuclear supernatant further was clarified at 10,000 × *g* for 10 min. The resulting supernatants were processed by another 100,000 × *g* centrifugation step for 1 h to collect a pellet (P3), typically enriched with small intracellular vesicles (5). Two- to 4-μg antibodies were coupled to magnetic Protein G Dynabeads (Invitrogen) at 4 °C for 4 h with constant rotating. Brain extracts from P3 fractions or HEK293 cell extracts were incubated with antibody-conjugated beads overnight, followed by extensive washing steps with IM-Ac buffer (20 mM Hepes, 100 mM KCl, 5 mM EGTA, and 5 mM $MgCl_2$ at pH 7.2) or IP buffer (150 mM NaCl, 50 mM Tris at pH 7.5, 5 mM $MgCl_2$), respectively, containing 0.5–1.0% Triton X-100. Bound proteins were eluted in SDS sample buffer, subjected to SDS/PAGE, and analyzed by Western blotting.

Vesicle Immunoisolation. Subcellular fractionation with subsequent immunopurification of vesicles carrying specific transmembrane proteins was performed as previously described (6, 7). In brief, whole mouse brains (P9-12) were homogenized in ice-cold sucrose buffer (320 mM sucrose, 10 mM Hepes, 5 mM EDTA at pH 7.3) freshly supplemented with protease inhibitor mixture (Roche) and 1 mM PMSF. Homogenates were centrifuged at 12,500 × *g* for 8 min, and the resulting supernatants were again centrifuged at 40,000 × *g* for 40 min. Next, supernatants were recovered and centrifuged at 120,000 × *g* for 1 h. The obtained pellet was resuspended in sucrose buffer and subjected to another centrifugation step at 120,000 × *g* for 1 h. To promote resuspension, the resulting pellet ($V1^C$) was vigorously stirred for 1 h before immunopurification. Dynabeads M280 sheep anti-mouse (Invitrogen) were washed twice with 0.1% BSA in PBS, incubated with antibodies (5 μg each in 0.1% BSA in PBS) for 1 h with constant rotating, and washed twice with 0.1% BSA in PBS, once with elution buffer (20 mM Tris at pH 7.4, 0.1% Triton X-100), and four times with IP buffer (PBS, 320 mM sucrose, 5 mM EDTA) supplemented with protease inhibitor mixture (Roche) and 1 mM PMSF. $V1^C$ vesicle fractions were incubated with antibody precoated beads for 2 h on a rotation wheel and washed 18–22 times with IP buffer. For electron microscopy studies, magnetic beads were collected by brief centrifugation, and the pellet was fixed in 4% (wt/vol) PFA and 0.1% (wt/vol) Glutaraldehyde in IP buffer. Further processing of beads was carried out as described in *SI Electron Microscopy*. For Western blot analysis without interfering with protein–protein interactions, beads were washed with 20 mM Tris at pH 7.4 and solubilized for 30 min in elution buffer before boiling in SDS sample buffer. For abrogation of protein–protein interactions, beads were additionally washed 3 times with 0.1 M Na_2CO_3 at pH 11 (8, 9), solubilized in elution buffer, and boiled in SDS sample buffer before SDS/PAGE and Western blotting.

Immunocytochemistry. Primary cultures of hippocampal neurons were prepared as described, and DIV11-15 neurons were fixed in 4% (wt/vol) PFA/4% (wt/vol) sucrose (10 min) and washed in PBS before permeabilization with 0.25% Triton X-100 (5 min). Unspecific binding sites were blocked with 3% (wt/vol) BSA (Applichem) for 1 h, and cells were incubated with primary antibodies overnight at 4 °C. Cells were washed three times in PBS and incubated with secondary antibodies for 1 h, washed extensively, and mounted in Aqua Poly Mount (Polysciences). For labeling surface populations of GluA2 containing AMPA-type glutamate receptors or *N*-cadherin, DIV11-13 hippocampal neurons were incubated with the respective primary antibodies (final concentrations as indicated in antibody section) for 2 h at 4 °C under nonpermeabilized conditions. Staining with secondary antibodies was carried out as described earlier. Microscopy analysis was carried out with an upright Laser-scanning Confocal Microscope Fluoview FV1000 with Olympus Fluoview Software Version 2.1.b (Olympus) or with an inverted Leica TCS-SP2 laser scanning confocal microscope (Leica Microsystems). For triple-labeling studies, a sequential scanning mode was used.

Electron Microscopy. Mice were deeply anesthetized and transcardially perfused with 4% (wt/vol) PFA and 0.1% (wt/vol) glutaraldehyde in phosphate buffer at pH 7.2. For postembedding immunogold labeling, small pieces of cryoprotected hippocampus (2.3 M sucrose) were mounted on specimen holders and immersed in liquid nitrogen. Ultrathin sections (70 nm) were then cut and labeled according to a previously described method (10).

Briefly, sections were collected on Carbon-Formvar-coated copper grids (Science Services GmbH). Antibodies, rabbit anti-GluA2 (1:100; Chemicon) and mouse anti-*N*-cadherin (1:100; BD Biosciences), were recognized with 10-nm and 15-nm large protein A gold secondary antibody, respectively (purchased from G. Posthuma, University Medical Center Utrecht). Similar results where achieved with mouse anti-GluA2 (1:100; Chemicon) and mouse anti-*N*-cadherin (1:100; BD Biosciences), which were sequentially applied, and each antibody was separately labeled with 10-nm and 15-nm large protein A gold particles, respectively. In parallel, four independent control labeling procedures were performed in which no antibody, rabbit anti-GluA2, mouse anti-GluA2 alone, or mouse anti-*N*-cadherin alone followed by 10-nm and 15-nm large protein A gold particles were applied. Ultrathin sections were examined, focusing on CA1 hippocampal neurons using a Zeiss EM 902 (Carl Zeiss). For quantitative studies only, rabbit anti-GluA2 and mouse anti-*N*-cadherin signals were analyzed. To this end, images of the Golgi apparatus were acquired, and the whole field of view at a 50,000× magnification was analyzed for 10-nm and 15-nm gold particles.

Surface Biotinylation Assay. HEK293 cells were transfected as described and, for 18 h posttransfection, were incubated for 20 min at 4 °C with Hepes buffer (135 mM NaCl, 5 mM KCl, 2 mM $CaCl_2$, 2 mM $MgCl_2$, 10 mM Hepes at pH 7.4, 15 mM glucose) containing 1 mM biotinamido-hexanoic acid 3-sulfo-*N*-hydroxysuccinimid-ester sodium salt (Sigma). For depolymerization of microtubules, 1 μM Nocodazole (Sigma) in 0.1% DMSO or 0.1% DMSO only was applied and incubated for 30 min at 37 °C before the biotin reagent was added. The remaining biotin reagent was quenched by application of 100 mM glycine in Hepes buffer (twice for 20 min at 4 °C).

Because low temperature is known to inhibit membrane trafficking and endocytosis, biotinylated cell surface expressed molecules remain at the plasma membrane during these incubations (11). Cells were then washed with ice-cold PBS and harvested in PBS containing 1% Triton X-100 with freshly added protease inhibitor mixture (Roche) and 1 mM PMSF. After 30 min of lysis on ice, followed by a brief centrifugation step at 1,000 × *g* (5 min, 4 °C), 30 μL of the supernatants were loaded on a gel to evaluate the total amount of *N*-cadherin or GluA2 posttransfection. In the case of equal *N*-cadherin or GluA2 total amounts, supernatants were added to 40 μL equilibrated magnetic streptavidin beads (Dynabeads Myone TM Streptavidin C1; Invitrogen). Beads were incubated with supernatants for 4 h at 4 °C on a rotation wheel, washed three times with IP buffer (150 mM NaCl, 50 mM Tris at pH 7.5, 5 mM $MgCl_2$) containing 1% Triton X-100, and collected and boiled in a SDS sample buffer before SDS/PAGE and Western blot analysis.

Time-Lapse Video Microscopy. Primary hippocampal neurons were prepared as described and cultured on 22-mm coverslips. Neurons were transfected at DIV10-11 through a calcium phosphate coprecipitation method, as described, and used for live cell imaging experiments at DIV13-14. Images were acquired at an upright microscope (Nikon Instruments) combined with Spinning Disk (Yokogawa) live cell confocal (SDC) technology (Visitron Systems). SDC was combined with two charge-coupled device electron microscopy cameras (Hamamatsu Photonics) and equipped with an optical image splitter for simultaneous dual image acquisition.

For single-channel live imaging (mRFP-NCAD), a 561-nm laser was used; images were taken at intervals of every 1 s for a duration of 5–10 min. For double-channel recordings (mRFP-NCAD and GFP-GluA2), 488-nm and 561-nm lasers were simultaneously used, and images were taken at intervals of every 3 s for a duration of 5 min. For image acquisition, a 60× objective (Nikon Instruments) was used. Cells at the microscope stage were kept in Primary Neuronal Basal Media (Lonza Group Ltd) and were temperature- (37 °C) and CO_2-controlled (5%), using a live imaging chamber (Visitron Systems). Images at the microscope stage were acquired using the VisiView software (Visitron Systems), and image stacks were subsequently loaded

into MetaMorph 7.1 (Universal Imaging) or Volocity 6.1.1 (Improvision; Perkin-Elmer) for analysis of fluorescent puncta. The percentage of mobile/immobile mRFP-NCAD particles on coexpression of GFP or GFP-KIF5CΔMD was calculated using manual and automated particle tracking analysis (Volocity 6.1.1) and normalized on the total amount of particles. For quantification of the percentages of cotransported GFP-GluA2/mRFP-NCAD, the number of mobile mRFP-NCAD particles that comigrated with GFP-GluA2 was divided by the total amount of mobile mRFP-NCAD particles. Tracking was performed by using MetaMorph 7.1 software (Universal Imaging), and cotransported particles were analyzed from image stacks and through manual analysis of the respective kymographs.

Image Processing and Statistical Analysis. For the evaluation of relative Western blot signal intensities, films were scanned with a resolution of 600 dpi, and signals were subsequently analyzed using the Image J, version 1.38, analysis software (National Institutes of Health). Signal intensities were then normalized compared with loading control signals for immunoblots. Statistical analysis was performed with SigmaPlot Version 10 (Systat Software Inc) and Microsoft Excel. Statistical significance was evaluated with the Student t test. All values from quantitative data are reported as mean ± SEM from n independent experiments. Error bars represent the SEM.

Fluorescence imaging was carried out with either an upright Laser-scanning Confocal Microscope Fluoview FV1000 with Olympus Fluoview Software Ver. 2.1.b (Olympus) or an inverted Leica TCS-SP2 laser scanning confocal microscope (Leica Microsystems), using a 63× objective. For simultaneous multiple-channel fluorescence, images were taken in a sequential channel recording mode. Confocal images from multiple individual cells used for statistical analysis were obtained using identical photomultiplier values throughout each experiment. All experiments were replicated at least three times, using different culture preparations.

Images were saved as overlay TIF-files and further processed off-line and analyzed using MetaMorph 7.1 (Universal Imaging). First, to differ between soma and neurites, regions of interest (ROIs) were defined throughout multiple image acquisition frames using the ROI tool. The overlay TIF files were then separated into green and red channels, using the color separate function, and ROIs were transferred from the overlay to each channel, using the transfer region function to define identical ROIs. For the definition of image thresholds, brightness was adjusted using the inclusive thresholding state function. Fluorescence intensity, size, and cluster number measurements were performed using the integrated morphometry analysis function within MetaMorph to assess the average signal intensity, total signal intensity, average cluster size, and cluster number of identically defined ROIs for each channel. Using the colocalization tool within Metamorph assessed the area of colocalization. For distribution studies, surface labeling analysis, or colocalization measurements, one or two neurites were randomly chosen from the distal parts of a neuron.

Statistical analysis was performed with SigmaPlot Version 10 (Systat Software Inc) and Microsoft Excel. Statistical significance was evaluated with the Student t test, according to the following definition: $P > 0.05$, not significant; $P = 0.01$–0.05, significant (*); $P = 0.001$–0.01, very significant (**); and $P < 0.001$, highly significant (***). All values from quantitative data are reported as mean ± SEM from n independent experiments. Error bars represent the SEM.

1. Osten P, et al. (2000) Mutagenesis reveals a role for ABP/GRIP binding to GluR2 in synaptic surface accumulation of the AMPA receptor. *Neuron* 27(2):313–325.
2. Dong H, et al. (1997) GRIP: A synaptic PDZ domain-containing protein that interacts with AMPA receptors. *Nature* 386(6622):279–284.
3. Heisler FF, et al. (2011) Muskelin regulates actin filament- and microtubule-based GABA(A) receptor transport in neurons. *Neuron* 70(1):66–81.
4. Maas C, et al. (2006) Neuronal cotransport of glycine receptor and the scaffold protein gephyrin. *J Cell Biol* 172(3):441–451.
5. Saito N, et al. (1997) KIFC2 is a novel neuron-specific C-terminal type kinesin superfamily motor for dendritic transport of multivesicular body-like organelles. *Neuron* 18(3):425–438.
6. Konecna A, et al. (2006) Calsyntenin-1 docks vesicular cargo to kinesin-1. *Mol Biol Cell* 17(8):3651–3663.
7. Steuble M, et al. (2010) Molecular characterization of a trafficking organelle: Dissecting the axonal paths of calsyntenin-1 transport vesicles. *Proteomics* 10(21):3775–3788.
8. Nakamura N, et al. (1995) Characterization of a cis-Golgi matrix protein, GM130. *J Cell Biol* 131(6 Pt 2):1715–1726.
9. Dirac-Svejstrup AB, Shorter J, Waters MG, Warren G (2000) Phosphorylation of the vesicle-tethering protein p115 by a casein kinase II-like enzyme is required for Golgi reassembly from isolated mitotic fragments. *J Cell Biol* 150(3):475–488.
10. Slot JW, Geuze HJ (2007) Cryosectioning and immunolabeling. *Nat Protoc* 2(10): 2480–2491.
11. Kittler JT, et al. (2004) Huntingtin-associated protein 1 regulates inhibitory synaptic transmission by modulating gamma-aminobutyric acid type A receptor membrane trafficking. *Proc Natl Acad Sci USA* 101(34):12736–12741.
12. Lu Q, et al. (1999) delta-catenin, an adhesive junction-associated protein which promotes cell scattering. *J Cell Biol* 144(3):519–532.
13. Simcha I, et al. (2001) Cadherin sequences that inhibit beta-catenin signaling: A study in yeast and mammalian cells. *Mol Biol Cell* 12(4):1177–1188.
14. Thoreson MA, et al. (2000) Selective uncoupling of p120(ctn) from E-cadherin disrupts strong adhesion. *J Cell Biol* 148(1):189–202.
15. Ozaki C, et al. (2010) p120-Catenin is essential for N-cadherin-mediated formation of proper junctional structure, thereby establishing cell polarity in epithelial cells. *Cell Struct Funct* 35(2):81–94.
16. Grigoriev I, et al. (2007) Rab6 regulates transport and targeting of exocytotic carriers. *Dev Cell* 13(2):305–314.
17. Dunn S, et al. (2008) Differential trafficking of Kif5c on tyrosinated and detyrosinated microtubules in live cells. *J Cell Sci* 121(Pt 7):1085–1095.
18. Maas C, et al. (2009) Synaptic activation modifies microtubules underlying transport of postsynaptic cargo. *Proc Natl Acad Sci USA* 106(21):8731–8736.
19. Thoumine O, Lambert M, Mège RM, Choquet D (2006) Regulation of N-cadherin dynamics at neuronal contacts by ligand binding and cytoskeletal coupling. *Mol Biol Cell* 17(2):862–875.
20. Shi SH (2001) Amersham Biosciences & Science Prize. AMPA receptor dynamics and synaptic plasticity. *Science* 294(5548):1851–1852.
21. Saglietti L, et al. (2007) Extracellular interactions between GluR2 and N-cadherin in spine regulation. *Neuron* 54(3):461–477.

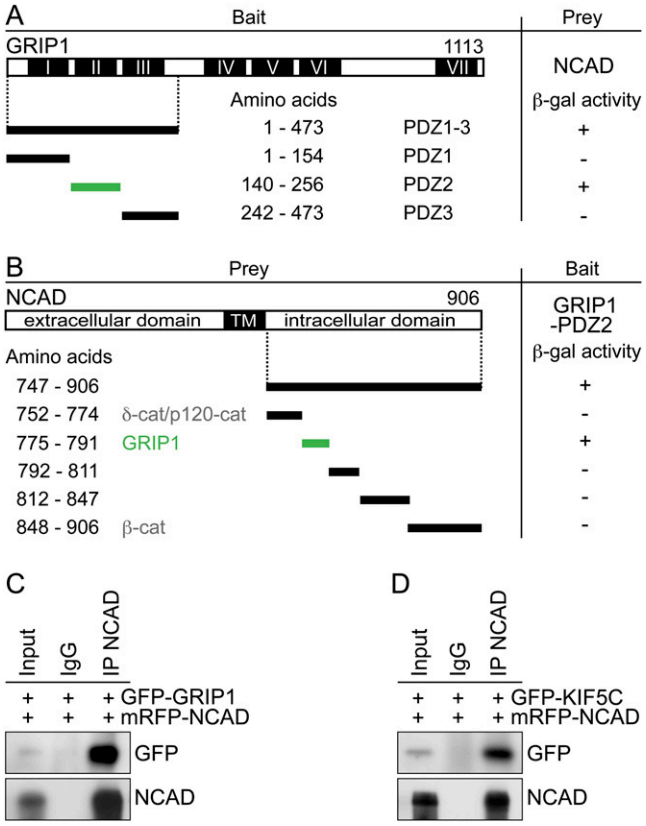

Fig. S1. *N*-cadherin directly interacts with GRIP1. (*A*) The domain architecture of the cargo adapter GRIP1 is shown. PDZ domains 1–3 of GRIP1 were used as bait for yeast two-hybrid screening. Two clones encoding aa102–906 of the cell adhesion molecule *N*-cadherin were identified. Deletion mutagenesis mapped PDZ2 of GRIP1 (aa140–256, green) as sufficient for NCAD binding. +, binding; -, no binding. (*B*) The domain architecture of *N*-cadherin is shown. The entire intracellular domain of NCAD (aa747–906) and five deletion constructs were generated for mapping the GRIP1-PDZ2 binding site on NCAD, using the yeast two-hybrid system. +, binding; -, no binding. Amino acids 775–791 of NCAD were identified for GRIP1-PDZ2 binding (green). Other reported binding sites of GRIP1-PDZ2 interaction partners (gray) (12–15) do not overlap with the NCAD binding site, as indicated. (*C*) Co-IP on expression of GFP-GRIP1 and mRFP-NCAD in HEK293 cells. NCAD-specific antibodies coprecipitate GFP-GRIP1. (*D*) Co-IP on expression of GFP-KIF5C and mRFP-NCAD in HEK293 cells. NCAD-specific antibodies coprecipitate GFP-KIF5C.

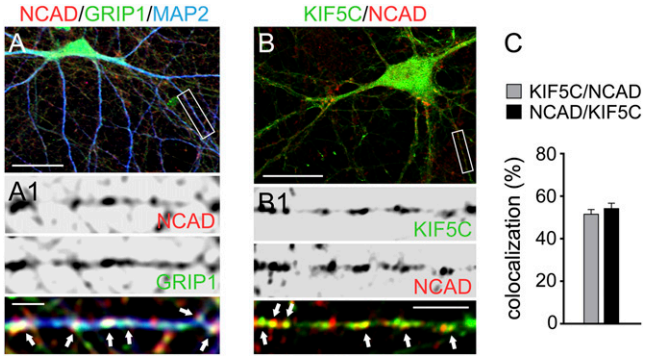

Fig. S2. *N*-cadherin colocalizes with GRIP1 and KIF5C in dendrites. (*A*–*C*) Immunostaining in DIV15 primary hippocampal neurons. Boxed regions are shown at higher magnification. (Scale bars, 30 μm in *A*, 25 μm in *B*, and 5 μm in *A1* and *B1*.) (*A*) Coimmunostaining with GRIP1-, NCAD-, and MAP2-specific antibodies detects colocalization within dendrites (arrows, MAP2-positive). (*B*) KIF5C and NCAD puncta colocalize within dendrite shafts on coimmunostaining (arrows). (*C*) Colocalization levels within dendrites: KIF5C over NCAD (51.86 ± 2.22) and NCAD over KIF5C (54.19 ± 2.40); 31 cells each.

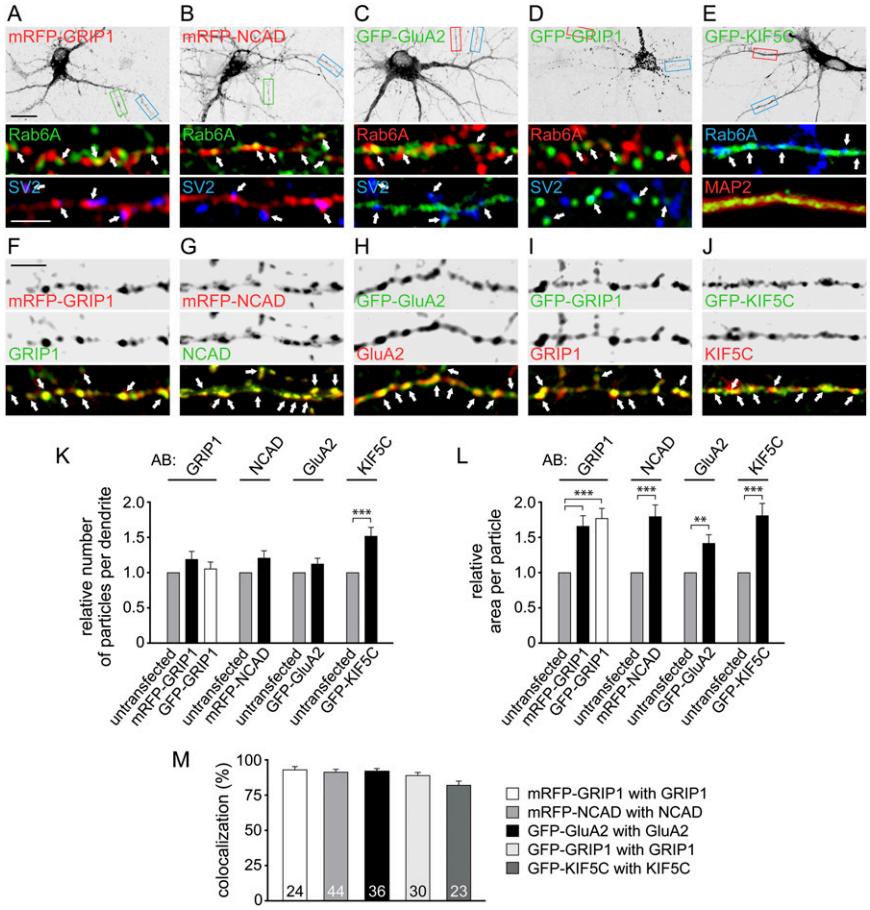

Fig. S3. Distribution of different fluorescent proteins (XFP)-fusion proteins in hippocampal neurons. (*A–E*) Primary hippocampal neurons, transfected with the indicated plasmids at DIV9-12, were allowed 18 h expression before immunostaining of Rab6A and SV2 (*A–D*) or Rab6A and MAP2 (*E*). Colocalization with SV2 indicates that XFP-fusions of GRIP1, NCAD, and GluA2 are frequently targeted to spine and shaft synapses (arrows). Rab6A was used to mark KIF5-driven Golgi-derived vesicles that traffic to the cell periphery (16). GFP-KIF5C and, notably, also the XFP-fusion proteins of GRIP1, NCAD, and GluA2 show a good degree of colocalization with Rab6A puncta (arrows), indicating that XFP-fusion proteins used in this study show an intracellular distribution similar to the endogenous proteins. Boxed regions are shown at higher magnification. (Scale bars, 20 μm for overviews and 5 μm for boxes.) (*F–J*) Hippocampal neurons, transfected at DIV9-12, were allowed 18 h expression of the indicated XFP-fusion proteins before immunostaining of their respective endogenous counterparts. High degrees of colocalization between the endogenous and XFP-fusion proteins used in this study are observed (arrows). Note that only a very few endogenous protein signals do not colocalize with their fusion protein counterpart. In addition to the controls provided here, other studies also reported a similar distribution of these XFP-fusion proteins compared with their endogenous counterparts (17–20). (Scale bar, 5 μm.) (*K* and *L*) Quantitative analysis of XFP-fusion protein distribution and expression compared with endogenous proteins. The relative numbers of particles per dendrite and the relative area per particle were compared between untransfected and transfected cells on immunostaining with antibodies (AB), as indicated. (*K*) The relative numbers of particles per dendrite segment are similar for most constructs between transfected and untransfected cells, suggesting a similar particle distribution. GRIP1 AB: mRFP-GRIP1, 1.19 ± 0.10 (23 cells); GFP-GRIP1, 1.04 ± 0.07 (28 cells); and untransfected, set to 1 (39 cells). NCAD AB: mRFP-NCAD, 1.21 ± 0.08 (48 cells), and untransfected, set to 1 (28 cells). GluA2 AB: GFP-GluA2, 1.12 ±0.05 (35 cells), and untransfected, set to 1 (33 cells). KIF5C AB: GFP-KIF5C, 1.53 ± 0.11 (23 cells), and untransfected, set to 1 (22 cells). (*L*) The relative areas per particles are increased in transfected compared with untransfected cells, indicative of overexpression of XFP-fusion proteins. GRIP1 AB: mRFP-GRIP1, 1.64 ± 0.14 (23 cells); GFP-GRIP1, 1.77 ± 0.12 (28 cells); and untransfected, set to 1 (39 cells). NCAD AB: mRFP-NCAD, 1.79 ± 0.13 (48 cells), and untransfected, set to 1 (28 cells). GluA2 AB: GFP-GluA2, 1.37 ± 0.11 (34 cells), and untransfected, set to 1 (33 cells). KIF5C AB: GFP-KIF5C, 1.81 ± 0.16 (23 cells), and untransfected, set to 1 (22 cells). (*M*) Quantitative analysis of colocalization levels between endogenous and XFP-fusion protein signals: mRFP-GRIP1 with GRIP1, 92.29 ± 1.88; mRFP-NCAD with NCAD, 90.26 ± 1.45; GFP-GluA2 with GluA2, 91.03 ± 1.18; GFP-GRIP1 with GRIP1, 89.17 ± 1.64; and GFP-KIF5C with KIF5C, 81.67 ± 2.29. Numbers of cells as indicated. Data are represented as mean ± SEM. The Student *t* test (***$P < 0.001$; **$P < 0.01$) was used for statistical analysis.

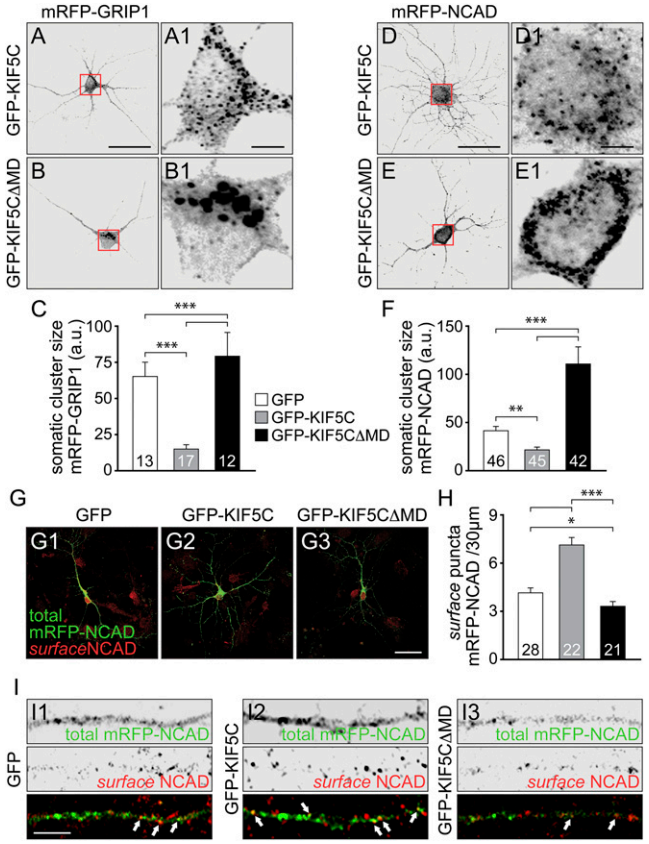

Fig. S4. GRIP1 and *N*-cadherin dendrite targeting depends on KIF5C. (*A*–*F*) Primary hippocampal neurons, transfected with plasmids encoding mRFP-GRIP1 or mRFP-NCAD at DIV9-12, were allowed 18 h expression before distribution analysis of newly synthesized mRFP-fusion particles. Boxed regions are shown at higher magnification. (Scale bars, 50 μm in *A*–*E* and 5 μm in *A1*–*E1*.) (*A* and *B*) Increased somatic mRFP-GRIP1 localization on GFP-KIF5CΔMD compared with GFP-KIF5C coexpression. (*C*) Quantitative analysis reveals decreased mRFP-GRIP1 somatic cluster sizes on GFP-KIF5C (14.90 ± 3.07) compared with GFP coexpressing control neurons (64.51 ± 10.10). GFP-KIF5CΔMD compared with GFP and GFP-KIF5C coexpression significantly increases average mRFP-GRIP1 somatic cluster sizes (78.78 ± 15.85). Numbers of cells as indicated. (*D* and *E*) mRFP-NCAD signals accumulate within the soma of GFP-KIF5CΔMD compared with GFP-KIF5C-expressing neurons. (*F*) Significantly decreased mRFP-NCAD cluster sizes are detected in GFP-KIF5C (22.10 ± 2.78) compared with GFP-coexpressing neurons (41.69 ± 4.41), whereas GFP-KIF5CΔMD coexpression increases somatic cluster sizes (110.28 ± 16.72). Numbers of cells as indicated. (*G*–*I*) Hippocampal neurons, transfected with mRFP-NCAD cDNA at DIV9-12, were allowed 18 h expression before surface immunostaining of NCAD. Total mRFP-NCAD and surface NCAD depicted in pseudocolor. (Scale bars, 50 μm in *G* and 5 μm in *I*). Overview of neurons (*G*) and single channels (*I*) of merge depicted in Fig. 2 *G*–*J* are shown. Arrows indicate surface mRFP-NCAD puncta (as judged by colocalization of total mRFP-NCAD with surface NCAD). (*H*) Please refer to legend in *C*. Numbers of newly synthesized mRFP-NCAD puncta at the cell surface per 30 μm dendrite segment are significantly increased on GFP-KIF5C (7.05 ± 0.33) and decreased after GFP-KIF5CΔMD (3.14 ± 0.29) compared with GFP (4.07 ± 0.24) coexpressing neurons. Numbers of cells as indicated. Data are represented as mean ± SEM. The Student *t* test (***$P < 0.001$; *$P < 0.05$) was used for statistical analysis.

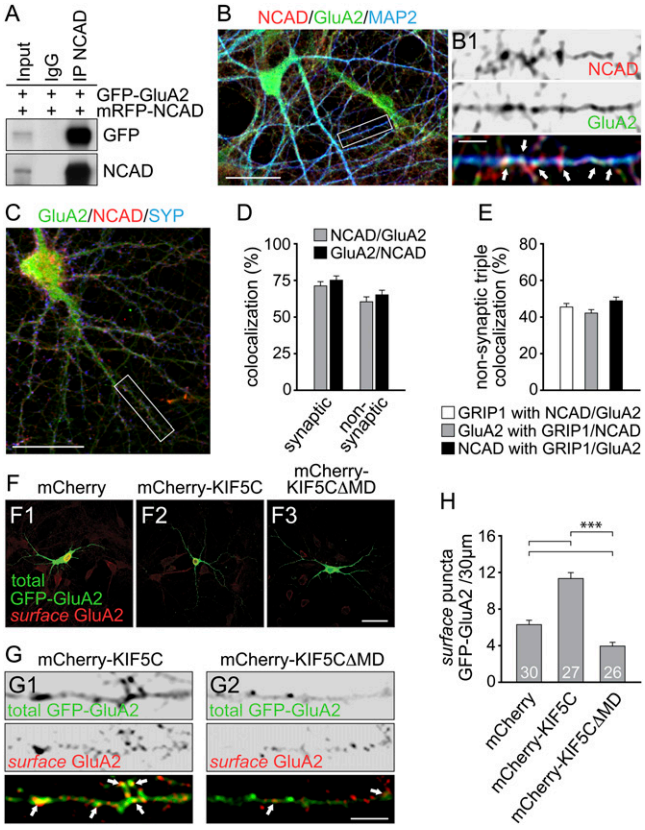

Fig. S5. GluA2 plasma membrane trafficking depends on KIF5C. (*A*) Co-IP of GFP-GluA2 with mRFP-NCAD from HEK293 cell lysates. Antibodies for precipitation as indicated on the top, for detection to the right. (*B*) Immunostaining in DIV15 primary hippocampal neurons. Boxed region is shown at higher magnification. (Scale bars, 30 μm in *B* and 5 μm in *B1*.) NCAD and GluA2 puncta frequently colocalize at MAP2-labeled dendrites (arrows). (*C* and *D*) Immunostaining in DIV15 hippocampal neurons detects colocalization of NCAD with GluA2 at dendrite shafts (Synaptophysin-negative; nonsynaptic) and at spine or shaft synapses (Synaptophysin-positive; synaptic). An overview of the cell corresponding to dendrite segments shown in Fig. 3*D* (boxed region) is depicted. (Scale bar, 25 μm in *D*.) Colocalization at synapses: NCAD over GluA2, 71.21 ± 2.98, and GluA2 over NCAD, 75.10 ± 2.98; nonsynaptic colocalization: NCAD over GluA2, 60.40 ± 3.39, and GRIP1 over NCAD, 65.10 ± 3.17; 44 cells each. (*E*) Quantification of immunostaining in DIV15 hippocampal neurons corresponding to dendrite segments shown in Fig. 3*E*. Only nonsynaptic sites were selected for colocalization analysis (negative for Synaptophysin immunostaining). GRIP1 with NCAD/GluA2, 45.66 ± 1.97; GluA2 with GRIP1/NCAD, 42.97 ± 2.06; and NCAD with GRIP1/GluA2, 47.47 ± 2.26; 44 cells each. (*F–H*) Hippocampal neurons, transfected with GFP-GluA2 cDNA at DIV9-12, were allowed 18 h expression before surface immunostaining of GluA2. Surface GluA2 is shown in pseudocolor. (Scale bars, 50 μm in *E* and 5 μm in *F*). Overview of neurons (*F*) and single channels (*G*) are shown at higher magnification. Arrows indicate surface GFP-GluA2 puncta (as judged by colocalization of total GFP-GluA2 with surface GluA2). (*H*) Numbers of newly synthesized GFP-GluA2 puncta at the cell surface per 30 μm dendrite segment are significantly increased on mCherry-KIF5C (11.41 ± 0.54) and decreased on mCherry-KIF5CΔMD (3.83 ± 0.22) compared with mCherry (6.30 ± 0.29) coexpressing neurons. Numbers of cells as indicated. Data are represented as mean ± SEM. The Student *t* test (***$P < 0.001$) was used for statistical analysis.

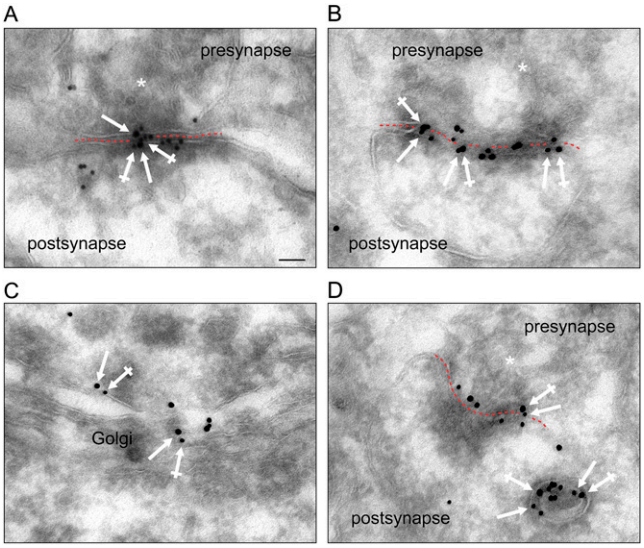

Fig. S6. *N*-cadherin and GluA2 are detected in close proximity at intracellular membranes. (*A–D*) Electron microscopy analysis of hippocampal tissue slices on double immunogold labeling, using NCAD and GluA2 specific antibodies. Crossed arrows indicate GluA2 signals [10-nm particles (*A* and *C*) and 15-nm particles (*B* and *D*)]; arrows mark NCAD signals [15-nm particles (*A* and *C*) and 10-nm particles (*B* and *D*)]. Asterisks indicate presynaptic terminals. Red dashed lines depict synaptic clefts. (Scale bar, 0.06 μm.) (*A* and *B*) Control showing the specificity of antibodies used. In agreement with previous studies, an accumulation of NCAD and GluA2 signals is detected at dendritic shaft (*A*) and spine synapses (*B*). Moreover, NCAD and GluA2 signals are detected in close proximity at the synaptic membrane (arrows, crossed arrows), confirming previous findings of direct NCAD/GluA2 interactions at excitatory synapses (21). (*C*) NCAD and GluA2 immunoreactivity is detected at intracellular membranes of the Golgi apparatus. Note that some of the NCAD/GluA2 signals are situated nearby each other (arrows, crossed arrows). (*D*) Spine synapse with an intracellular vesicle at the postsynaptic compartment. NCAD/GluA2 signals are detected at the synaptic membrane. In addition, the vesicle membrane harbors several NCAD and GluA2 signals in close proximity (arrows, crossed arrows).

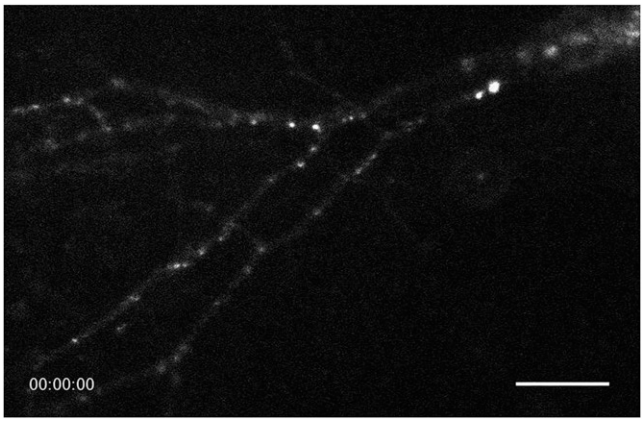

Movie S1. Mobility of mRFP-NCAD particles on GFP coexpression (control) in DIV13 hippocampal neurons. The mRFP-NCAD signal is shown. Image acquisition intervals were 1 s over the duration of 2:10 min. The movie plays with 30 frames per second. (Scale bar, 12 μm.)

Movie S1

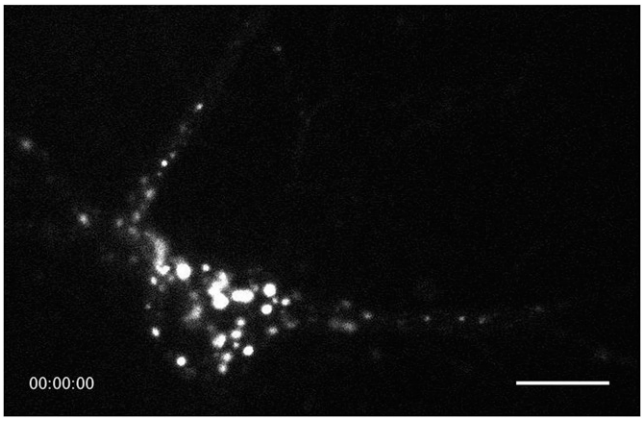

Movie S2. Mobility of mRFP-NCAD particles on interference with KIF5C-based transport through GFP-KIF5CΔMD coexpression in DIV13 hippocampal neurons. The mRFP-NCAD signal is shown. Image acquisition intervals were 1s over the duration of 2:10 min. The movie plays with 30 frames per second. (Scale bar, 12 μm.)

Movie S2

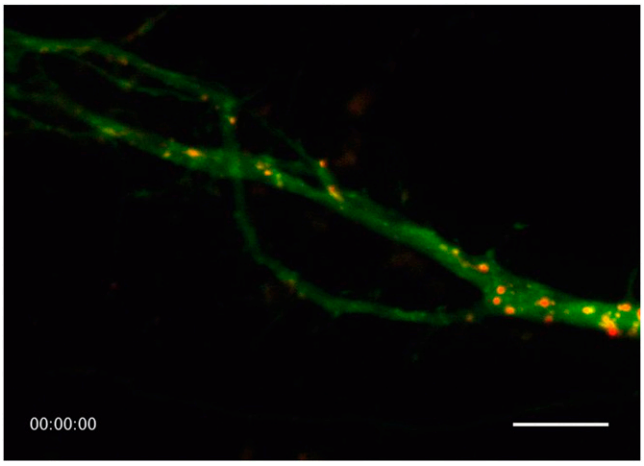

Movie S3. Subpopulations of mRFP-NCAD (red) and GFP-GluA2 (green) particles undergo combined vesicle transport (yellow particles) in DIV 13 hippocampal neurons. Note that smaller cotransport packets are frequently mobile, whereas larger colocalized puncta mainly remain immobile. Image acquisition intervals were 3 s over the duration of 05:00 min. The movie plays with 30 frames per second. (Scale bar, 12 μm.)

Movie S3